AJNR

SWI by 7T MR Imaging for the Microscopic Imaging Diagnosis of Astrocytic and Oligodendroglial Tumors

M. Natsumeda, H. Matsuzawa, M. Watanabe, K. Motohashi, R. Gabdulkhaev, Y. Tsukamoto, Y. Kanemaru, J. Watanabe, R. Ogura, M. Okada, S. Kurabe, K. Okamoto, A. Kakita, H. Igarashi and Y. Fujii

SWI by 7T MR Imaging for the Microscopic Imaging Diagnosis of Astrocytic and Oligodendroglial Tumors

M. Natsumeda, H. Matsuzawa, M. Watanabe, K. Motohashi, R. Gabdulkhaev, Y. Tsukamoto, Y. Kanemaru, J. Watanabe, R. Ogura, M. Okada, S. Kurabe, K. Okamoto, A. Kakita, H. Igarashi, and Y. Fujii

ABSTRACT

BACKGROUND AND PURPOSE: Despite advances in molecular imaging, preoperative diagnosis of astrocytomas and oligodendrogliomas can be challenging. In the present study, we assessed whether 7T SWI can be used to distinguish astrocytomas and oligodendrogliomas and whether malignant grading of gliomas is possible.

MATERIALS AND METHODS: 7T SWI was performed on 21 patients with gliomas before surgery with optimization for sharp visualization of the corticomedullary junction. Scoring for cortical thickening and displacement of medullary vessels, characteristic of oligodendroglial tumors, and cortical tapering, characteristic of astrocytic tumors, was performed. Additionally, characteristics of malignancy, including thickening of the medullary veins, the presence of microbleeds, and/or necrosis were scored.

RESULTS: Scoring for oligodendroglial (highest possible score, $+3$) and astrocytic (lowest score possible, -3) characteristics yielded a significant difference between astrocytomas and oligodendrogliomas (mean, -1.93 versus $+1.71$, $P < .01$). Scoring for malignancy was significantly different among the World Health Organization grade II ($n = 10$), grade III ($n = 4$), and grade IV ($n = 7$) tumors (mean, 0.20 versus 1.38 versus 2.79). Cortical thickening was observed significantly more frequently in oligodendrogliomas ($P < .02$), with a sensitivity of 71.4% and specificity of 85.7%; observation of tapering of the cortex was higher in astrocytomas ($P < .01$) with a sensitivity of 85.7% and specificity of 100%.

CONCLUSIONS: Visualization of the corticomedullary junction by 7T SWI was useful in distinguishing astrocytomas and oligodendrogliomas. Observation of tapering of the cortex was most sensitive and specific for diagnosing astrocytomas. Reliably predicting malignant grade was also possible by 7T SWI.

ABBREVIATIONS: GRE = gradient recalled-echo; LIV = local image variance; WHO = World Health Organization; IDH = isocitrate dehydrogenase

Recent molecular analyses have greatly advanced our ability to pathologically diagnose gliomas. Isocitrate dehydrogenase (*IDH*) mutation in the absence of 1p/19q codeletion is diagnostic for astrocytomas, and *IDH* mutation with 1p/19q codeletion, for oligodendrogliomas.[1]

However, radiographically distinguishing astrocytomas and oligodendrogliomas remains challenging by conventional MR imaging. Features such as calcification and lower homogeneous signal on T2WI are characteristic for 1p/19q-codeleted oligodendrogliomas, whereas the presence of T2 FLAIR mismatch and subventricular zone invasion is characteristic of 1p/19q-noncodeleted, *IDH*-mutant astrocytomas.[2,3] MR perfusion studies have suggested that higher maximum relative CBV[4] and lower extravascular extracellular distribution volume (V_e) values, especially in conjunction with calcification and high cortical involvement, are suggestive of oligodendroglioma.[5] MR spectroscopy studies revealed that the metabolites mIns-to-Cr ratio was significantly higher in astrocytomas compared with oligodendrogliomas.[6] Furthermore, MR imaging texture analysis[7] and radiomics[8] were applied to reliably distinguish astrocytomas and oligodendrogliomas. Molecular imaging of gliomas has also entered the era of clinical application. The detection of the oncometabolite 2-hydroxyglutarate by MR spectroscopy has made accurate, presurgical diagnosis of *IDH*-mutant gliomas possible.[9-11] A recent MR spectroscopy study suggested that cystathionine is a marker for oligodendrogliomas with 1p/19q codeletion,[12] though more robust methods are desired.

Marked improvements in the contrast-to-noise ratio by 7T MR imaging has enabled visualization of high-resolution images. Seminal work by Duyn et al[13] used gradient recalled-echo (GRE) MR imaging and a multichannel detector to achieve a nominal voxel size of $0.24 \times 0.24 \times 1.0$ mm^3 (58 nL). We have previously described the microscopic application of 7T MR imaging by postprocessing of T2* GRE images to depict senile plaquelike structures in Alzheimer disease.[14] By means of this method, visualization of the corticomedullary junction,[15] medullary vessels, and microbleeds was possible, aiding in the diagnosis of gliomas. Especially, the visualization of the corticomedullary junction and fine medullary vessels is not possible by 3T MR imaging. Here, we report for the first time, the usefulness of 7T SWI for the preoperative diagnosis of astrocytomas and oligodendrogliomas, as well as malignant grading.

MATERIALS AND METHODS
Patients
Twenty-one adult patients with World Health Organization (WHO) grade II–IV gliomas, including 13 (61.9%) patients with relatively small (diameter of <3 cm) gliomas localized to the cortical and/or subcortical area, undergoing 7T MR imaging evaluation at the Center for Integrated Brain Science, Niigata University before surgical treatment at the Department of Neurosurgery, Niigata University between April 2009 and December 2015 were included in the study. Written informed consent was obtained from all participants in accordance with the human research guidelines of the internal review board of Niigata University (approval # H16-263).

7T MR Imaging. SWI studies were performed using a 7T Signa Horizon LX (GE Healthcare) MR imaging system. Details of the clinical microscopic imaging techniques used were previously described.[16-18]

High-resolution T2*-weighted 2D GRE images were obtained with TR = 220 ms, TE = 21.4 ms, flip angle = 20°, FOV = 80 × 80 mm, and matrix size = 512 × 512 with 3-mm thickness (0.156 × 0.156 × 3 mm in spatial resolution) (Online Supplemental Data). SWIs were obtained by postprocessing of T2*-weighted 2D GRE images, adhering to methods originally introduced by Reichenbach et al[19] using in-house software written in MATLAB (MathWorks) on a Windows-based computer (Online Supplemental Data).[20]

To determine the optimal postprocessing parameters for assessment of gliomas, we altered the kernel size of the filter sequentially from 4 to 255 (Online Supplemental Data) and the number of phase mask multiplications from 0 to 54 (Online Supplemental Data). A kernel size filter of 64 was determined to be optimal for phase unwrapping (Online Supplemental Data) and the number of phase mask multiplications to optimize the contrast-to-noise ratio 9 times (Online Supplemental Data) for the visualization of veins running inside the tumor. Thus, the optimal parameters to visualize gliomas were the same as those previously reported for microscopic imaging of senile plaquelike structures in patients with Alzheimer disease.[14]

Pathologic Diagnosis
Surgical specimens were independently analyzed by 2 pathologists (R.G. and A.K.) and diagnosed according to the WHO 2016 classification.[21] Differences in diagnosis (mainly judgments between

WHO grades II and III) in a couple of cases were resolved by deliberation. IDH1 R132H (H09 clone, Dianova, 1:100), ATRX (polyclonal, SIGMA-Aldrich; 1:1000), and P53 (clone DO-7; Dako Omnis; 1:50) immunohistochemical analysis was performed in formalin-fixed, paraffin-embedded sections using the avidin-biotin-peroxide method (Vectorlabs) with diaminobenzidine as the chromogen and counterstained with hematoxylin.[22]

For cases showing negative staining for IDH1 R132H, DNA sequencing for *IDH1* and *IDH2* was analyzed. Methods for sequencing are specified in the Online Supplemental Data.

Assessment of 1p/19q Codeletion
Methods for assessment of 1p/19q codeletion are detailed in the Online Supplemental Data.

Assessment of 7T Imaging
One experienced neuroradiologist (K.O.) and a neurosurgeon (M.N.) independently assessed 7T SWIs, blinded to the clinical information. Thickening of the cortex, assessed by an increase of the distance from the cortical surface to the corticomedullary junction by ≥50% (scored +1 present/–1 absent) and displacement of medullary vessels (scored +1 present/–1 absent) were considered characteristic of oligodendrogliomas. The tapering or thinning of the corticomedullary junction was considered characteristic of astrocytomas (scored −1 present/+1 absent). Therefore, a minimum score of −3 (astrocytoma-like) and maximum score of +3 (oligodendroglioma-like) were assessed. Findings for malignancy were also scored. The thickening of the medullary veins and the presence of microbleeds and/or necrosis were each scored as +1 when present, zero when absent. Thus, a minimum score of zero and a maximum score of +3 were possible. Scores were presented as means (SD). To calculate the sensitivity and specificity of specific categories, the 2 scorers resolved interobserver variability by thorough discussion.

Statistical Analyses
Differences between 2 groups were assessed by an unpaired *t* test, differences among 3 groups were assessed by the 1-way ANOVA test with the post hoc Tukey multiple comparison test, and contingency tables were assessed by the Fisher exact test using GraphPad Prism 9 software (GraphPad Software). Error bars represent standard error of the mean unless otherwise specified. $P < .05$ was considered statistically significant.

RESULTS
Optimization of SWI
After optimization, the visualization of the corticomedullary junction, seen as a hypointense band (triangles), and elongation of the medullary vessels running perpendicular to the cortical surface (brackets) were clearly depicted by 7T SWI (Fig 1A). This detail cannot be achieved by SWI (Fig 1B), T1-weighted (Fig 1C), or FLAIR imaging (Fig 1D) using a conventional 3T machine. Additionally, 7T SWIs appeared to show higher resolution than 3T SWIs (Online Supplemental Data), though specific parameters differed.
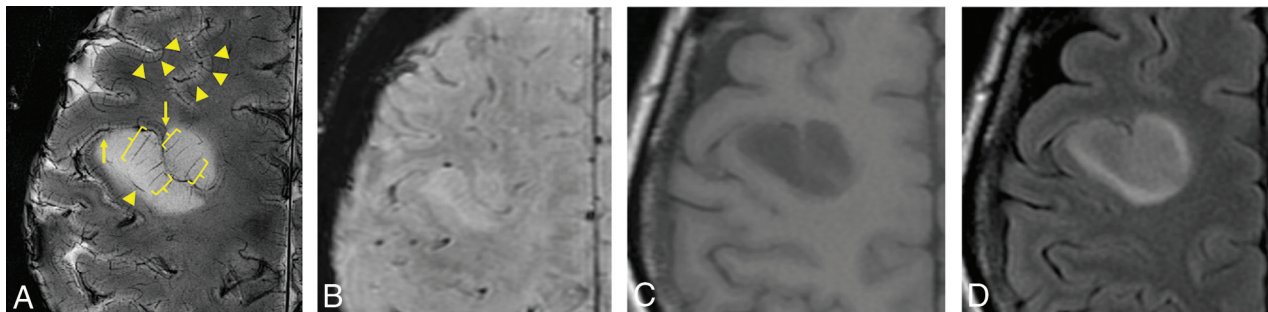
FIG 1. Comparison of 7T SWI and 3T MR imaging. Displacement of the corticomedullary junction, seen as a hypointense band (*triangles*), and elongation of medullary veins running perpendicular to the cortical surface (*brackets*) can be observed on 7T SWI (spatial resolution, 0.156 × 0.156 × 3 mm; total scan time, 3 minutes and 48 seconds; number of slices, 5) (*A*), which cannot be appreciated on 3T SWI (0.653 × 0.653 × 2 mm; 4 minutes and 12 seconds; 64 slices) (*B*), 3T T1-weighted images (*C*), or 3T FLAIR images (*D*) obtained on a 3T clinical scanner. Apparent cortical thickening was observed in this diffuse astrocytoma, giving the impression of an oligodendroglioma. However, on close inspection, tapering of the cortex is observed at the edges of the lesion (*A*, *arrows*).
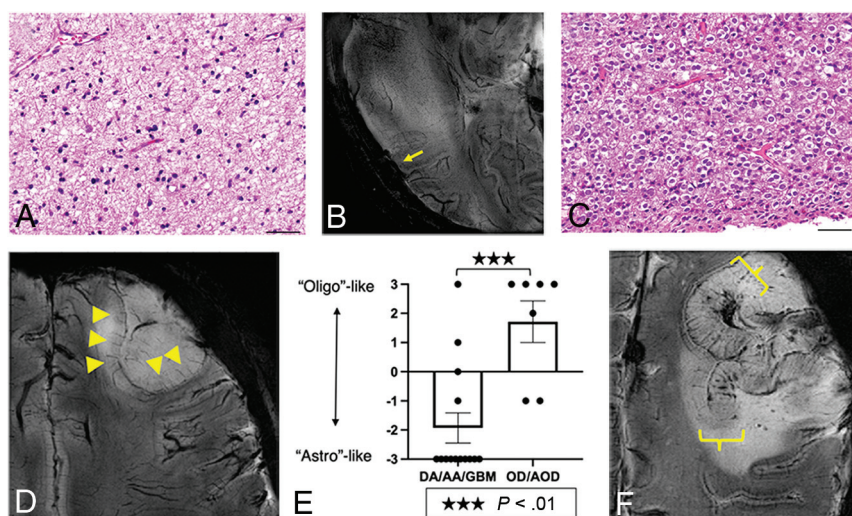

FIG 2. 7T SWI characteristics of astrocytic and oligodendroglial lesions. Astrocytic lesions (*A*) were predominantly located in the WM and displayed infiltrative growth and focal obscuring of the corticomedullary junction (*arrow*) without displacing medullary vessels and other normal structures on 7T SWI (*B*). An oligodendroglioma (WHO grade II) with classic perinuclear halos and chicken wire-like vessels (*C*) shows thickening of the cortex (*triangles*), elongation but not thickening of the medullary vessels of the cortex, and expansive growth, displacing the medullary vessels on 7T-SWI (*D*). Scoring yielded a significant difference between astrocytomas and oligodendrogliomas (mean −1.93 versus +1.71, *P* < .01) (*E*). In a case of anaplastic oligodendroglioma, *IDH*-mutant and 1p/19q-codeleted, diffuse thickening of the cortex without tapering, thickening of medullary vessels, and microbleeds were observed (*F*). Scale bars = 50 µm. DA/AA/GBM indicates diffuse astrocytoma/anaplastic astrocytoma/glioblastoma; OD/AOD, oligodendroglioma/anaplastic oligodendroglioma.

Pathologic Diagnosis

Demographics, pathologic diagnoses, and molecular profiles of the 21 patients with gliomas are summarized in the Online Supplemental Data. The age of patients ranged from 29 to 81 years (median, 50 years); 10 female patients and 11 male patients were recruited. Tumors in 7 of 21 (33%) patients were pathologically diagnosed as WHO grade IV; 4 (19%), as WHO grade III; and 10 (48%), as grade II. The *IDH1* R132H mutation was detected in 12 (57%) tumors; *IDH2* R172W, in 1 (5%) tumor; and the rest (38%) were *IDH1/2* wild-type. The 1p/19q codeletion was detected by fluorescence in site hybridization in 7 (33%) cases and thus these were diagnosed as

oligodendroglioma. In 1 diffuse astrocytoma, an *IDH*-mutant case, 1p was intact but 19q loss was detected (Online Supplemental Data).

Scoring for Astrocytic and Oligodendroglial Characteristics

A representative astrocytic tumor (Fig 2A) showed predominant WM invasion without massive cortical involvement and focal disappearance of the corticomedullary junction (Fig 2B, arrow). Hypointensities reflecting normal vascular structures were not displaced and/or became less obvious, reflecting the invasive nature of astrocytomas. Oligodendrogliomas (Fig 2C), on the other hand, showed cortical involvement with likely cortical thickening, elongation of cortical medullary vessels, and displacement of vascular structures, evidence of expansive growth (Fig 2D). Scoring for these characteristics yielded a significant difference between astrocytomas and oligodendrogliomas (mean −1.93 [SD, 0.10] versus +1.71 [SD, 0.20], *P* < .001, Fig 2E).

We next looked at the sensitivity and specificity of each characteristic to diagnose oligodendrogliomas and astrocytomas. Cortical thickening was found in 5 of 7 (71.4%) oligodendrogliomas, whereas only 2 of 14 (14.3%) astrocytomas showed this feature (*P* < .02). Therefore, observation of cortical thickening yielded a sensitivity of 71.4% and specificity of 85.7% for diagnosing oligodendrogliomas. Likewise, displacement of medullary vessels was found in 4 of 7 (57.1%) oligodendrogliomas but in only 3 of 14 (21.4%) astrocytomas (*P* = .16), thus yielding a sensitivity of 57.1% and specificity of 78.6% for diagnosing oligodendrogliomas. Finally, observation of tapering of the cortex, suggesting invasion of the tumor from the WM into the cortex, was found in 12 of 14
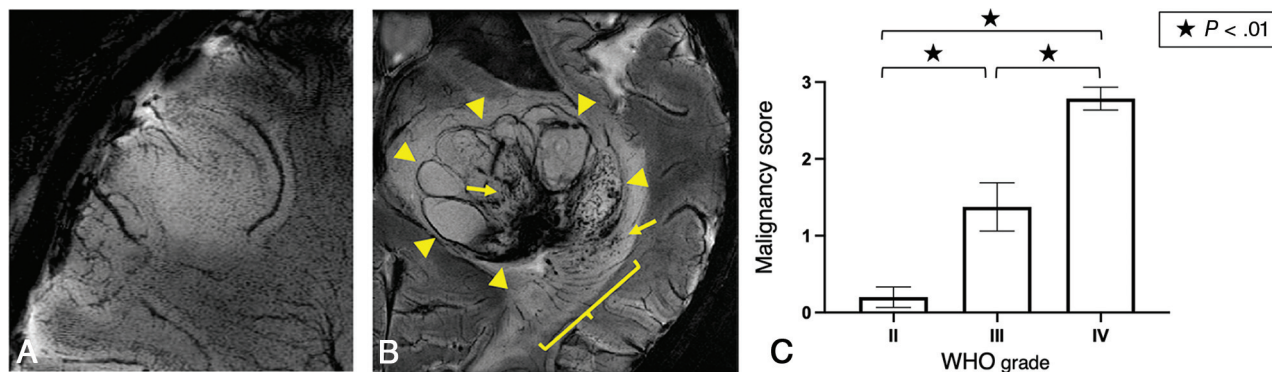
FIG 3. Malignancy scoring of gliomas. A diffuse astrocytoma, *IDH* mutant (WHO grade II) with a malignancy score of 0 (*A*), and a glioblastoma, *IDH* wild-type (WHO grade IV) with a malignancy score of 3, with evidence of thickening of medullary vessels (*bracket*), microbleeds (*arrows*) and necrosis (surrounded by *triangles*) (*B*). Malignancy scoring was significantly elevated in WHO grade III tumors compared with grade II (mean, 1.38 versus 0.20, $P < .01$), and grade IV tumors compared with grade III (mean, 2.79 versus 1.38, $P < .01$) and grade II ($P < .01$) (*C*).
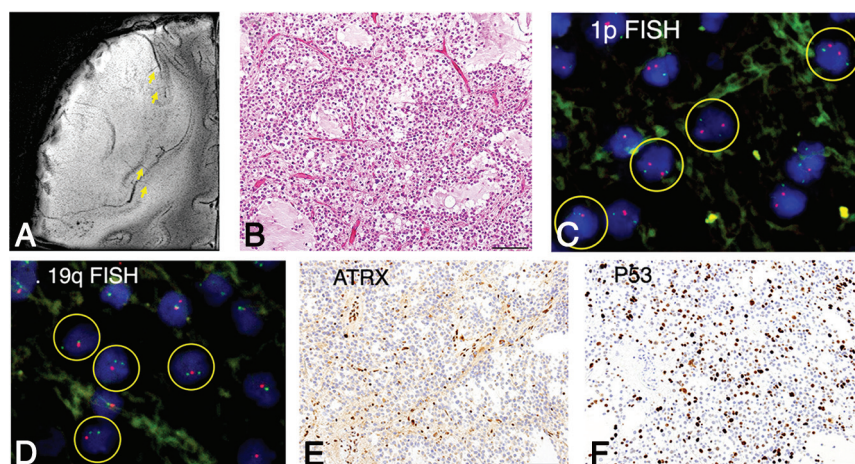

FIG 4. A diffuse astrocytoma, *IDH*-mutant, displaying thickening of the cortex with elongation of medullary vessels (*arrows*) and expansive growth on 7T MR imaging, mimicking an oligodendroglioma (*A*). Morphologically, the tumor displayed predominantly oligodendroglioma-like pathology (*B*). Fluorescence in situ hybridization (FISH) revealed 1p-intact (*C*), 19q-loss (*D*). ATRX staining was lost in tumor cells (*E*), and P53 was immunopositive (>10% positive) (*F*), suggesting astrocytic lineage. Scale bars = 100 µm. *Circles* indicate individual tumor cells.

II) assessed as zero points (Fig 3*A*) and a glioblastoma, *IDH* wild-type (WHO grade IV) scored as 3 points (Fig 3*B*) for malignancy are presented. Scoring was significantly different among WHO grade II (diffuse astrocytomas and oligodendrogliomas, $n = 10$), grade III (anaplastic astrocytoma and anaplastic oligodendrogliomas, $n = 4$), and grade IV (glioblastomas, $n = 7$) tumors (mean, 0.20 [SD, 0.0] versus 1.38 [SD, 0.18] versus 2.79 [SD, 0.10], Fig 4*C*) (II versus III $P < .01$; III versus IV $P < .01$; and II versus IV $P < .01$). Most interesting, all 4 WHO grade II oligodendrogliomas had a malignancy score of zero, whereas WHO grade III anaplastic oligodendrogliomas were scored as 1.5 or 2 (mean, 1.67, $P < .03$) (Online Supplemental Data). Notably, thickening of medullary vessels was observed in all WHO grade III anaplastic oligodendrogliomas (Fig 2*F*), but in none of the WHO grade II oligodendrogliomas (Fig 2*D*) ($P < .03$).

Diffuse Astrocytoma Displaying Radiographic and Pathologic Features of Oligodendroglioma
One astrocytoma had radiographic characteristics of cortical thickening without tapering and displacement of medullary vessels, characteristic of oligodendrogliomas (Fig 4*A*). Hence, the scoring was +3. Close pathologic examination revealed that the tumor itself had predominant, morphologic characteristics of oligodendroglioma (Fig 4*B*). The 1p/19q analysis revealed 19q loss, but 1p was intact (Fig 4*C*, -*D*). Most interesting, ATRX immunostaining was lost (Fig 4*E*) and P53 staining was positive (Fig 4*F*) in tumor cells, suggestive of *IDH*-mutant astrocytoma.

DISCUSSION
In the present report, we show, for the first time, that 7T SWI is useful in distinguishing astrocytic and oligodendroglial tumors.

(85.7%) astrocytomas, but in none of the 7 (0%) oligodendrogliomas ($P < .01$) that showed diffuse thickening of the cortex. Therefore, this observation yielded a sensitivity of 85.7% and specificity of 100% in diagnosing astrocytomas. In a case of a relatively small cortical-subcortical tumor, elongation of medullary vessels in the cortex and distinct borders were observed, giving the impression of an oligodendroglioma (Fig 1*A*). However, observation of the corticomedullary junction demonstrated tapering of the cortex at the edges (Fig 1*A*, arrows), suggesting invasion of a subcortical tumor into the cortex, and pathologic diagnosis was diffuse astrocytoma, *IDH*-mutant. In a pathologically confirmed anaplastic oligodendroglioma, *IDH*-mutant and 1p/19q-codeleted, diffuse cortical thickening without tapering was observed (Fig 2*F*, brackets).

Scoring for Malignancy
Scoring for malignancy was performed by detection of microbleeds, thickening of medullary veins, and/or necrosis. An oligodendroglioma, *IDH*-mutant and 1p/19q-codeleted (WHO grade

Very fine details such as thickening and displacement of medullary vessels and disruption and displacement of the corticomedullary junction, which are not readily detected by 3T SWI, were observed by 7T MR microscopy. This method was especially useful in the diagnosis of small gliomas located in cortical/subcortical areas. We found that thickening of the cortex and elongation of corticomedullary vessels and displacement of medullary vessels and other normal structures were suggestive of oligodendroglial tumors, with a few exceptions. On the other hand, tapering of the cortex and latency of medullary vessels were characteristic of astrocytic tumors.

Astrocytomas with Oligodendroglioma-like Characteristics

We found 1 case showing cortical involvement and expansive growth on 7T SWI (Fig 4A) and displaying a predominant oligodendroglioma-like morphology (Fig 4B). However, surrogate markers including ATRX loss and P53 immunopositivity suggested astrocytic tumor, and 1p/19q fluorescence in site hybridization indicated that 1p was intact, though 19q was lost. Otani et al[23] reported 7 cases of IDH-mutant and 1p-intact/19q-loss anaplastic astrocytomas, containing areas of oligodendroglioma-like morphology with longer survival compared with 19q-intact anaplastic astrocytomas. Radiographic features of these tumors were not mentioned in the report. The presence of such cases that would be diagnosed as IDH-mutant, 1p/19q-noncodeleted astrocytomas but possessing oligodendroglioma-like features may confound the radiographic diagnosis of astrocytic-versus-oligodendroglial tumors.

7T SWI for Determination of Malignant Grade. Furthermore, we found that detection of microbleeds, thickened medullary vessels, and/or necrosis was suggestive of malignant tumors. Massive necrosis can often be observed by 1.5 or 3T MR imaging, but microbleeds can be difficult to distinguish from blood vessels or small necrosis, and medullary vessels cannot readily be observed even on postcontrast images. Medullary vessels were clearly depicted on 7T SWI without the use of contrast media. Most interesting, all 4 WHO grade II oligodendrogliomas had a malignancy score of zero, whereas none of the 3 WHO grade III anaplastic oligodendrogliomas had a malignancy score of zero. Notably, thickening of the medullary vessels was observed in all WHO grade III oligodendrogliomas, whereas none of the WHO grade II oligodendrogliomas showed thickening ($P < .03$). A recent article suggests the difficulty of differentiating WHO grade II and III oligodendrogliomas by conventional T1 contrast-enhanced and FLAIR images.[24] Di Ciantis et al[25] showed that in 6 of 21 (29%) patients with intractable epilepsy with conventional MRIs with unrevealing findings, structural lesions were found by 7T 2D GRE. Further investigation is needed, but 7T SWI may detect vessel changes and small microbleeds not observed on conventional MR imaging.

Interpreting the Findings on 7T SWI in Gliomas

In the present report, we found 7T SWI to be useful in distinguishing oligodendrogliomas and astrocytomas and high susceptibility correlated with malignancy. Susceptibility is most likely affected by venous structures within the tumor, microbleeds, as well as iron and calcium deposition. When one pathologically diagnoses gliomas, not much attention is given to venous structures within the tumor. Detailed assessment of venous structures within gliomas may lead to a better understanding of the intensities found on 7T SWI microscopy.

Application of 7T SWI in Assessment of Brain Tumors and Other Diseases

Reports of 7T SWI for radiographic assessment of brain tumors have largely been restricted to small reports.[26] An important study by Grabner et al[27] showed that local image variance (LIV) or quantification of hypointensities on 7T SWI was higher in 21 high-grade gliomas compared with 9 low-grade gliomas and that significantly higher values were found in IDH1-R132H-negative gliomas compared with IDH1-R132H-positive ones. Evidently, the results of LIV SWI correspond with malignancy scores in the present article, being higher in higher-grade gliomas. Correlation of LIV SWI and IDH mutation can be interpreted as follows: A high percentage of lower-grade gliomas exist in IDH-mutant cases, whereas IDH wild-type gliomas are likely to be glioblastomas. Di Ieva et al[28] reported the usefulness of fact-based quantification as a robust method of assessing signal heterogeneity on 7T SWI to analyze tumor grade in gliomas, in agreement with results of the malignancy score in the present study.

Other 7T SWI reports exist of visualization of vascular anomalies such as cavernous malformations with associated developmental venous anomalies,[29,30] radiation-induced microbleeds,[31-33] iron deposition in multiple sclerosis lesions,[34-36] substantia nigra in Parkinson disease,[37] other degenerative diseases,[38] and senile plaquelike lesions in patients with Alzheimer disease.[14] In the present study, we found that the same postprocessing methods were optimal for visualization of the corticomedullary junction and the small vasculature of gliomas.

Limitations

Study limitations include the small sample size, selection bias restricting eligible patients to those demonstrating mild or no symptoms to eliminate motion artifacts during long imaging times, lack of direct comparison between 7T SWI and 3T SWI in this series, the use of a semiquantitative scoring system that requires subjective judgment, difficulty of generalizing to clinical practice because of limited accessibility to 7T scanners, the use of a deliberately tailored protocol using 7T SWI with limited brain coverage, and the unavailability of multiparametric 7T data such as enhancement and diffusion restriction due to time constraints.

CONCLUSIONS

Despite recent advances, the preoperative diagnosis of gliomas remains challenging. In the present report, we performed 7T SWI in a series of 21 patients with gliomas and found a close correlation between findings of cortical thickening and displacement of medullary vessels on 7T SWI with oligodendrogliomas, whereas cortical tapering and infiltrative expansion in the WM was found in astrocytomas. Tapering of the cortex was associated with the highest sensitivity and specificity in distinguishing astrocytomas from oligodendrogliomas. Additionally, observations of thickening of medullary vessels, microbleeds, and necrosis were associated with a higher WHO grade. 7T SWI is a useful tool to distinguish

astrocytomas and oligodendrogliomas and to determine malignancy in these tumors.

REFERENCES

1. Ohgaki H, Kleihues P. **Genetic profile of astrocytic and oligodendroglial gliomas.** *Brain Tumor Pathol* 2011;28:177–83 CrossRef Medline

2. Zhao K, Sun G, Wang Q, et al. **The diagnostic value of conventional MRI and CT features in the identification of the IDH1-mutant and 1p/19q co-deletion in WHO grade II gliomas.** *Acad Radiol* 2021;28:e189–98 CrossRef Medline

3. Broen MP, Smits M, Wijnenga MM, et al. **The T2-FLAIR mismatch sign as an imaging marker for non-enhancing IDH-mutant, 1p/19q-intact lower-grade glioma: a validation study.** *Neuro Oncol* 2018; 20:1393–99 CrossRef Medline

4. Cha S, Tihan T, Crawford F, et al. **Differentiation of low-grade astrocytomas by using quantitative blood-volume measurements derived from dynamic susceptibility contrast-enhanced MR imaging.** *AJNR Am J Neuroradiol* 2005;26:266–73 Medline

5. Yoon HJ, Ahn KJ, Lee S, et al. **Differential diagnosis of oligodendroglial and astrocytic tumors using imaging results: the added value of perfusion MR imaging.** *Neuroradiology* 2017;59:665–75 CrossRef Medline

6. Chawla S, Oleaga L, Wang S, et al. **Role of proton magnetic resonance spectroscopy in differentiating oligodendrogliomas from astrocytomas.** *J Neuroimaging* 2010;20:3–8 CrossRef Medline

7. Zhang S, Chiang GC, Magge RS, et al. **MRI based texture analysis to classify low grade gliomas into astrocytoma and 1p/19q codeleted oligodendroglioma.** *Magn Reson Imaging* 2019;57:254–58 CrossRef Medline

8. Shofty B, Artzi M, Ben Bashat D, et al. **MRI radiomics analysis of molecular alterations in low-grade gliomas.** *Int J Comput Assist Radiol Surg* 2018;13:563–71 CrossRef Medline

9. Choi C, Ganji SK, DeBerardinis RJ, et al. **2-hydroxyglutarate detection by magnetic resonance spectroscopy in IDH-mutated patients with gliomas.** *Nat Med* 2012;18:624–29 CrossRef Medline

10. Natsumeda M, Igarashi H, Nomura T, et al. **Accumulation of 2-hydroxyglutarate in gliomas correlates with survival: a study by 3.0-Tesla magnetic resonance spectroscopy.** *Acta Neuropathol Commun* 2014;2:158 CrossRef Medline

11. Natsumeda M, Motohashi K, Igarashi H, et al. **Reliable diagnosis of IDH-mutant glioblastoma by 2-hydroxyglutarate detection: a study by 3-T magnetic resonance spectroscopy.** *Neurosurg Rev* 2018;41:641–47 CrossRef Medline

12. Branzoli F, Pontoizeau C, Tchara L, et al. **Cystathionine as a marker for 1p/19q codeleted gliomas by in vivo magnetic resonance spectroscopy.** *Neuro Oncol* 2019;21:765–74 CrossRef Medline

13. Duyn JH, van Gelderen P, Li TQ, et al. **High-field MRI of brain cortical substructure based on signal phase.** *Proc Natl Acad Sci U S A* 2007;104:11796–801 CrossRef Medline

14. Nakada T, Matsuzawa H, Igarashi H, et al. **In vivo visualization of senile-plaque-like pathology in Alzheimer's disease patients by MR microscopy on a 7T system.** *J Neuroimaging* 2008;18:125–29 CrossRef Medline

15. Nakada T, Matsuzawa H, Igarashi H, et al. **Expansion of corticomedullary junction high-susceptibility region (CMJ-HSR) with aging: a clue in the pathogenesis of Alzheimer's disease?** *J Neuroimaging* 2012;22:379–83 CrossRef Medline

16. Kabasawa H, Nabetani A, Matsuzawa H, et al. **Imaging optimization for in-vivo human micro imaging at 7T.** In: *Proceedings of the International Society for Magnetic Resonance in Medicine*, Vancouver, British Columbia, Canada. April 12–18, 2006

17. Nakada T, Nabetani A, Kabasawa H, et al. **The passage to human MR microscopy.** *Magn Reson Med Sci* 2005;4:83–87 CrossRef Medline

18. Nakada T. **Clinical application of high and ultra-high-field MRI.** *Brain Dev* 2007;29:325–35 CrossRef Medline

19. Reichenbach JR, Barth M, Haacke EM, et al. **High-resolution MR venography at 3.0 Tesla.** *J Comput Assist Tomogr* 2000;24:949–57 Medline

20. Haacke EM, Xu Y, Cheng YC, et al. **Susceptibility weighted imaging (SWI).** *Magn Reson Med* 2004;52:612–18 CrossRef Medline

21. Louis DN, Ohgaki H, Wiestler OD, et al. *WHO Classification of Tumors of the Central Nervous System.* International Agency for Research on Cancer; 2016

22. Ogura R, Tsukamoto Y, Natsumeda M, et al. **Immunohistochemical profiles of IDH1, MGMT and P53: practical significance for prognostication of patients with diffuse gliomas.** *Neuropathology* 2015; 35:324–35 CrossRef Medline

23. Otani R, Uzuka T, Higuchi F, et al. **IDH-mutated astrocytomas with 19q-loss constitute a subgroup that confers better prognosis.** *Cancer Sci* 2018;109:2327–35 CrossRef Medline

24. Zhao SS, Feng XL, Hu YC, et al. **Better efficacy in differentiating WHO grade II from III oligodendrogliomas with machine-learning than radiologist's reading from conventional T1 contrast-enhanced and fluid attenuated inversion recovery images.** *BMC Neurol* 2020;20:48 CrossRef Medline

25. De Ciantis A, Barba C, Tassi L, et al. **7T MRI in focal epilepsy with unrevealing conventional field strength imaging.** *Epilepsia* 2016; 57:445–54 CrossRef Medline

26. Moenninghoff C, Kraff O, Schlamann M, et al. **Assessing a dysplastic cerebellar gangliocytoma (Lhermitte-Duclos disease) with 7T MR imaging.** *Korean J Radiol* 2010;11:244–48 CrossRef Medline

27. Grabner G, Kiesel B, Wohrer A, et al. **Local image variance of 7 Tesla SWI is a new technique for preoperative characterization of diffusely infiltrating gliomas: correlation with tumour grade and IDH1 mutational status.** *Eur Radiol* 2017;27:1556–67 CrossRef Medline

28. Di Ieva A, God S, Grabner G, et al. **Three-dimensional susceptibility-weighted imaging at 7 T using fractal-based quantitative analysis to grade gliomas.** *Neuroradiology* 2013;55:35–40 CrossRef Medline

29. Frischer JM, God S, Gruber A, et al. **Susceptibility-weighted imaging at 7 T: improved diagnosis of cerebral cavernous malformations and associated developmental venous anomalies.** *Neuroimage Clin* 2012;1:116–20 CrossRef Medline

30. Dammann P, Wrede KH, Maderwald S, et al. **The venous angioarchitecture of sporadic cerebral cavernous malformations: a susceptibility weighted imaging study at 7 T MRI.** *J Neurol Neurosurg Psychiatry* 2013;84:194–200 CrossRef Medline

31. Lupo JM, Chuang CF, Chang SM, et al. **7-Tesla susceptibility-weighted imaging to assess the effects of radiotherapy on normal-appearing brain in patients with glioma.** *Int J Radiat Oncol Biol Phys* 2012;82:e493–500 CrossRef Medline

32. Bian W, Banerjee S, Kelly DA, et al. **Simultaneous imaging of radiation-induced cerebral microbleeds, arteries and veins, using a multiple gradient echo sequence at 7 Tesla.** *J Magn Reson Imaging* 2015;42:269–79 CrossRef

33. Morrison MA, Mueller S, Felton E, et al. **Rate of radiation-induced microbleed formation on 7T MRI relates to cognitive impairment in young patients treated with radiation therapy for a brain tumor.** *Radiother Oncol* 2021;154:145–53 CrossRef Medline

34. Haacke EM, Makki M, Ge Y, et al. **Characterizing iron deposition in multiple sclerosis lesions using susceptibility weighted imaging.** *J Magn Reson Imaging* 2009;29:537–44 CrossRef Medline

35. Louapre C, Treaba CA, Barletta V, et al. **Ultra-high field 7 T imaging in multiple sclerosis.** *Curr Opin Neurol* 2020;33:422–29 CrossRef Medline

36. Filippi M, Evangelou N, Kangarlu A, et al. **Ultra-high-field MR imaging in multiple sclerosis.** *J Neurol Neurosurg Psychiatry* 2014;85:60–66 CrossRef Medline

37. Cosottini M, Frosini D, Pesaresi I, et al. **MR imaging of the substantia nigra at 7 T enables diagnosis of Parkinson disease.** *Radiology* 2014;271:831–38 CrossRef Medline

38. Johns SLM, Ishaque A, Khan M, et al. **Quantifying changes on susceptibility weighted images in amyotrophic lateral sclerosis using MRI texture analysis.** *Amyotroph Lateral Scler Frontotemporal Degener* 2019;20:396–403 CrossRef Medline